

The cylindrical K -function and Poisson line cluster point processes

Jesper Møller*, Farzaneh Safavimanesh† and Jakob G. Rasmussen‡

Department of Mathematical Sciences, Aalborg University, Denmark

Abstract

Analyzing point patterns with linear structures has recently been of interest in e.g. neuroscience and geography. To detect anisotropy in such cases, we introduce a functional summary statistic called the cylindrical K -function. A class of models for anisotropic spatial point processes, called Poisson line cluster point processes, is also introduced. Parameter estimation based on moment methods or Bayesian inference for this model is discussed when the underlying Poisson line process and the cluster memberships are treated as hidden processes. To illustrate the methodologies, we analyze two and three-dimensional point pattern data sets.

Keywords: anisotropy, Bayesian inference, directional K -function, minicolumn hypothesis, Poisson line process, three-dimensional point pattern analysis.

1 Introduction

Frequently in the spatial point process literature, isotropy (i.e. distributional invariance under rotations about a fixed location in space) is assumed for convenience, though it is often realized that it may be an unrealistic assumption. Anisotropy of spatial point processes has been studied various places in the literature, usually by summarizing the information of observed pairs of points, including the use of directional K -functions or related densities (Ohser and Stoyan, 1981; Stoyan and Beneš, 1991; Stoyan, 1991; Stoyan and Stoyan, 1995; Redenbach *et al.*, 2009), spectral and wavelet methods (Mugglestone and Renshaw, 1996; Rosenberg, 2004); (Nicolis, Mateu and Dercole, 2010), and geometric anisotropic pair correlation functions (Møller and Toftaker, 2014). The applications considered in these references except Redenbach *et al.* (2009) are only for 2D and not 3D point patterns. This paper focuses on detecting and modelling anisotropy caused by linear structures in spatial point patterns observed within a bounded subset of \mathbb{R}^d , $d \geq 2$, where the cases $d = 2$ and $d = 3$ are of main interest. For this we need to develop a new directional K -function and new statistical models.

Section 2 introduces the cylindrical K -function, a directional K -function whose structuring element is a cylinder which is suitable for detecting anisotropy e.g. caused by a linear structure in a spatial point pattern. In fact it is an adapted version of the space-time K -function (Diggle *et al.*, 1995; Gabriel and Diggle, 2009). Section 3 concerns a new class of point processes, called Poisson line cluster point processes, since the points cluster around a hidden Poisson line process, and discusses a simulation-based approach for Bayesian inference. The

*jm@math.aau.dk (corresponding author)

†farzaneh@math.aau.dk

‡jgr@math.aau.dk

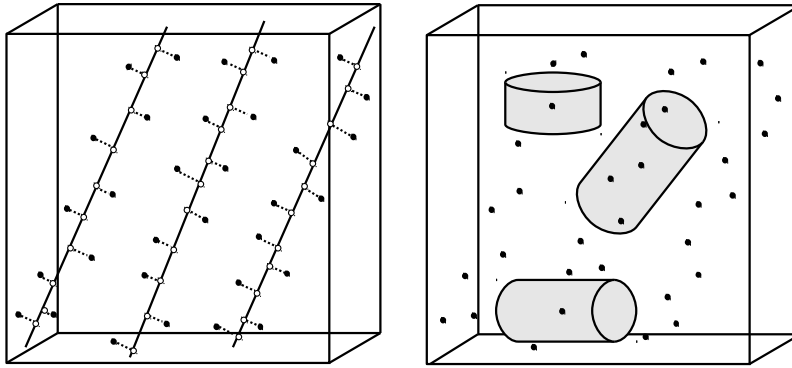


Figure 1: Left panel: A simulated realization of a Poisson line cluster point process within a 3D box. The realizations of the hidden Poisson line process and the hidden Poisson point processes on the lines are also shown. The dotted lines indicate how the hidden points have been displaced and they specify the clusters. Right panel: The same simulated realization of a Poisson line cluster point process and different choices of cylinders centered at different points of the process.

left panel in Figure 1 illustrates how such a process is constructed: Lines are generated from an anisotropic Poisson line process (the solid lines), independent stationary Poisson point processes are generated on the lines (the circles), and their points are randomly displaced, resulting in the Poisson line cluster point process (the filled circles). We treat the Poisson lines and the points on the lines as hidden processes. Thus also the clusters of the Poisson line cluster point process (specified by the dotted lines in the figure) are hidden.

Sections 2-3 apply our methodology for the data sets in Figure 2. The left panel shows a 2D point pattern data set recorded by Mugglestone and Renshaw (1996), namely the locations of 110 chapels in the Welsh Valleys, United Kingdom, where the clear linear orientation is caused by four more or less parallel valleys. The right panel shows an example of a 3D point pattern data set, namely the locations of 623 pyramidal cells from the Brodmann area 4 of the grey matter of the human brain (collected by the neuroscientists at the Center for Stochastic Geometry and Bioimaging, Denmark). According to the minicolumn hypothesis (Mountcastle, 1957), brain cells (mainly pyramidal cells) should have a columnar arrangement perpendicular to the pial surface of the brain, and this should be highly pronounced in Brodmann area 4. However, this hypothesis has been much debated, see Rafati *et al.* (2015) and the references therein.

While we use the chapel data set mainly for illustrative purposes and for comparison with previous work, investigations of the minicolumn hypothesis have so far only been done in 2D except for the 3D analysis in Rafati *et al.* (2015) which relies on the methodology developed in this paper. Moreover, this paper provides a more thorough analysis of the pyramidal cell data set.

2 The cylindrical K -function

Section 2.1 specifies the setting used in this paper, Section 2.2 introduces the cylindrical K -function and discusses its properties, Section 2.3 shows how it can be estimated non-parametrically taking boundary effects into account, and Section 2.4 discusses its applications for the data sets in Figure 2.

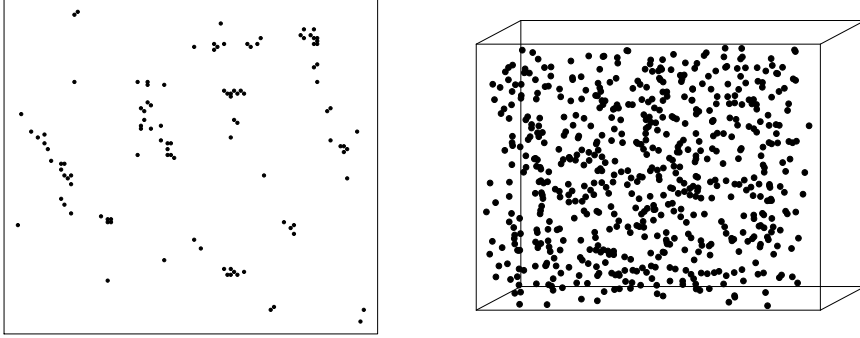


Figure 2: Left panel: Locations of 110 chapels in Wales, United Kingdom, observed in a square window (normalized to a unit square). Right panel: Nucleolus of 623 pyramidal cells in an observation window of size $508 \times 138 \times 320 \mu\text{m}^3$.

2.1 Setting

Throughout this paper we make the following assumptions and use the following notation.

We consider a stationary point process \mathbf{X} defined on \mathbb{R}^d , with finite and positive intensity ρ , and where we view \mathbf{X} as a locally finite random subset of \mathbb{R}^d . Here stationarity means that the distribution of \mathbf{X} is invariant under translations in \mathbb{R}^d , and $\rho|B|$ is the mean number of points from \mathbf{X} falling in any Borel set $B \subseteq \mathbb{R}^d$ of volume $|B|$. We assume that \mathbf{X} has a so-called pair correlation function $g(\mathbf{x})$ defined for all $\mathbf{x} \in \mathbb{R}^d$. Intuitively, if $\mathbf{x}_1, \mathbf{x}_2 \in \mathbb{R}^d$ are distinct locations and B_1, B_2 are infinitesimally small sets of volumes $d\mathbf{x}_1, d\mathbf{x}_2$ and containing $\mathbf{x}_1, \mathbf{x}_2$, respectively, then $\rho^2 g(\mathbf{x}_1 - \mathbf{x}_2) d\mathbf{x}_1 d\mathbf{x}_2$ is the probability for \mathbf{X} having a point in each of B_1 and B_2 . For further details on spatial point processes, see Møller and Waagepetersen (2004) and the references therein.

We view any vector $\mathbf{x} = (x_1, \dots, x_d) \in \mathbb{R}^d$ as a column vector, and $\|\mathbf{x}\| = (x_1^2 + \dots + x_d^2)^{1/2}$ as its usual length. For ease of presentation, we assume that no pair of distinct points $\{\mathbf{x}_1, \mathbf{x}_2\} \subset \mathbf{X}$ is such that $\mathbf{u} = (\mathbf{x}_1 - \mathbf{x}_2)/\|\mathbf{x}_1 - \mathbf{x}_2\|$ is perpendicular to the x_d -axis. This will happen with probability one for the specific models considered later in this paper.

Let $\mathbb{S}^{d-1} = \{\mathbf{u} = (u_1, \dots, u_d) \in \mathbb{R}^d : \|\mathbf{u}\| = 1\}$ be the unit-sphere in \mathbb{R}^d and $\mathbf{e}_d = (0, \dots, 0, 1)$ its ‘top point’. Denote $\mathbf{o} = (0, \dots, 0)$ the origin of \mathbb{R}^d . Consider the d -dimensional cylinder with midpoint \mathbf{o} , radius $r > 0$, height $2t > 0$, and direction \mathbf{e}_d :

$$C(r, t) = \{\mathbf{x} = (x_1, \dots, x_d) \in \mathbb{R}^d : x_1^2 + \dots + x_{d-1}^2 \leq r^2, |x_d| \leq t\}.$$

For $\mathbf{u} \in \mathbb{S}^{d-1}$, denoting $\mathcal{O}(\mathbf{u})$ an arbitrary $d \times d$ rotation matrix such that $\mathbf{u} = \mathcal{O}_{\mathbf{u}}\mathbf{e}_d$, then

$$C_{\mathbf{u}}(r, t) = \mathcal{O}_{\mathbf{u}}C(r, t)$$

is the d -dimensional cylinder with midpoint \mathbf{o} , radius r , height $2t$, and direction \mathbf{u} .

2.2 Definition of the cylindrical K -function

Recall that the second order reduced moment measure \mathcal{K} with ‘structuring element’ $B \subset \mathbb{R}^d$ (a bounded Borel set) is given by

$$\mathcal{K}(B) = \int_B g(\mathbf{x}) \, d\mathbf{x}$$

(see e.g. Section 4.1.2 in Møller and Waagepetersen (2004)). Ripley’s K -function (Ripley, 1976, 1977) is obtained when B is a ball and it is not informative about any kind of anisotropy in a spatial point pattern. Directional K -functions have been suggested using a sector annulus (Ohser and Stoyan, 1981) or a double cone (Redenbach *et al.*, 2009). To detect preferred directions of linear structures in a spatial point pattern, we use a cylinder as the structuring element and define the *cylindrical K -function in the direction \mathbf{u}* by

$$K_{\mathbf{u}}(r, t) = \int_{C_{\mathbf{u}}(r, t)} g(\mathbf{x}) \, d\mathbf{x}, \quad \mathbf{u} \in \mathbb{S}^{d-1}, \, r > 0, \, t > 0. \quad (1)$$

Intuitively, $\rho K_{\mathbf{u}}(r, t)$ is the mean number of further points in \mathbf{X} within the cylinder with midpoint at the ‘typical point’ of \mathbf{X} , radius r , and height $2t$ in the direction \mathbf{u} . For example, a stationary Poisson process is isotropic, has $g = 1$, and

$$K_{\mathbf{u}}(r, t) = 2\omega_{d-1}r^{d-1}t$$

where $\omega_{d-1} = \pi^{(d-1)/2}/\Gamma((d+1)/2)$ is the volume of the $(d-1)$ -dimensional unit ball.

For $d = 3$, $K_{(0,0,1)}$ is similar to the space-time K -function in Diggle *et al.* (1995) and Gabriel and Diggle (2009), when considering the x_3 -axis as time and the (x_1, x_2) -plane as space. Let $W \subset \mathbb{R}^d$ denote an arbitrary Borel set with $0 < |W| < \infty$. Then an equivalent definition is

$$K_{\mathbf{u}}(r, t) = \frac{1}{\rho^2|W|} \mathbb{E} \sum_{\mathbf{x}_1, \mathbf{x}_2 \in \mathbf{X}: \mathbf{x}_1 \neq \mathbf{x}_2} \mathbf{1}[\mathbf{x}_1 \in W, \mathbf{x}_2 - \mathbf{x}_1 \in C_{\mathbf{u}}(r, t)], \quad r > 0, \, t > 0, \quad (2)$$

where $\mathbf{1}[\cdot]$ denotes the indicator function. This definition does not require the existence of the pair correlation function, and it does not depend on the choice of W , since \mathbf{X} is stationary. Equation (2) becomes useful when deriving non-parametric estimates in Section 2.3.

2.2.1 Inhomogeneous case

In some applications (not considered in this paper) it is relevant to use a non-constant intensity function $\rho(\mathbf{x})$. Suppose we assume second order intensity reweighted stationarity (Baddeley, Møller and Waagepetersen, 2000) and $g(\mathbf{x})$ still denotes the pair correlation function. This means intuitively, if $\mathbf{x}_1, \mathbf{x}_2 \in \mathbb{R}^d$ are distinct locations and B_1, B_2 are infinitesimally small sets of volumes $d\mathbf{x}_1, d\mathbf{x}_2$ and containing $\mathbf{x}_1, \mathbf{x}_2$, respectively, then $\rho(\mathbf{x}_1)\rho(\mathbf{x}_2)g(\mathbf{x}_1 - \mathbf{x}_2)d\mathbf{x}_1d\mathbf{x}_2$ is the probability for \mathbf{X} having a point in each of B_1 and B_2 . Our definition (1) still applies, while (2) becomes

$$K_{\mathbf{u}}(r, t) = \frac{1}{|W|} \mathbb{E} \sum_{\mathbf{x}_1, \mathbf{x}_2 \in \mathbf{X}: \mathbf{x}_1 \neq \mathbf{x}_2} \frac{\mathbf{1}[\mathbf{x}_1 \in W, \mathbf{x}_2 - \mathbf{x}_1 \in C_{\mathbf{u}}(r, t)]}{\rho(\mathbf{x}_1)\rho(\mathbf{x}_2)}, \quad r > 0, \, t > 0,$$

which in turn can be used when deriving non-parametric estimates.

2.3 Non-parametric estimation

Given a bounded observation window $W \subset \mathbb{R}^d$ and an observed point pattern $\{\mathbf{x}_1, \dots, \mathbf{x}_n\} \subset W$ with $n \geq 2$ points, we consider non-parametric estimates of the form

$$\hat{K}_{\mathbf{u}}(r, t) = \frac{1}{\hat{\rho}^2} \sum_{i \neq j} w_{\mathbf{u}}(\mathbf{x}_i, \mathbf{x}_j) \mathbf{1}[\mathbf{x}_j - \mathbf{x}_i \in C_{\mathbf{u}}(r, t)]. \quad (3)$$

Here $\hat{\rho}^2$ is a non-parametric estimate of ρ^2 and $w_{\mathbf{u}}$ is an edge correction factor. If \mathbf{X} is isotropic, $K_{\mathbf{u}}(r, t)$ is not depending on \mathbf{u} and this should be reflected when considering $\hat{K}_{\mathbf{u}}(r, t)$. On the other hand, as illustrated in the right panel of Figure 1 and in Section 2.4, to detect a preferred direction of linearity in a spatial point pattern, we suggest using an elongated cylinder (i.e. $t > r$) and considering different directions \mathbf{u} . Then we expect a largest value of $\hat{K}_{\mathbf{u}}(r, t)$ to indicate the preferred direction, but a careful choice of r and t may be crucial, cf. the discussion in Safavianesh and Redenbach (2015). Furthermore, since $K_{\mathbf{u}} = K_{-\mathbf{u}}$, we need only to consider the case where $\mathbf{u} = (u_1, \dots, u_d)$ is on the upper unit-sphere (i.e. $u_d \geq 0$).

Specifically, we use $\hat{\rho}^2 = n(n-1)/|W|^2$ (see e.g. Illian *et al.* (2008)) and the translation correction factor (Ohser and Stoyan, 1981)

$$w_{\mathbf{u}}(\mathbf{x}_1, \mathbf{x}_2) = 1/|W \cap W_{\mathbf{x}_2 - \mathbf{x}_1}| \quad (4)$$

where $W_{\mathbf{x}}$ denotes translation of the set W by a vector $\mathbf{x} \in \mathbb{R}^d$. Then, by Lemma 4.2 in Møller and Waagepetersen (2004), if $\hat{\rho}^2$ is replaced by ρ^2 in (3), we have an unbiased estimate of $K_{\mathbf{u}}$. As in Figures 1-2, if W is rectangular with sides parallel to the axes and of lengths $a_1, \dots, a_d > 0$,

$$|W \cap W_{\mathbf{x}_2 - \mathbf{x}_1}| = \prod_{i=1}^d (a_i - |x_{2,i} - x_{1,i}|), \quad \mathbf{x}_1, \mathbf{x}_2 \in W,$$

where $x_{j,i}$ denotes the i 'th coordinate of \mathbf{x}_j , $j = 1, 2$.

For $d = 3$, $W = [0, a_1] \times [0, a_2] \times [0, a_3]$, and $\mathbf{u} = (0, 0, 1)$, another choice is a combined correction factor

$$w_{(0,0,1)}(\mathbf{x}_1, \mathbf{x}_2) = \frac{1 + \mathbf{1}[2x_{2,3} - x_{1,3} \notin [0, a_3]]}{a_3(a_1 - |x_{2,1} - x_{1,1}|)(a_2 - |x_{2,2} - x_{1,2}|)}$$

where the numerator is a temporal correction factor and the denominator is the reciprocal of a spatial correction factor (similarly we construct combined correction factors when $\mathbf{u} = (1, 0, 0)$ or $\mathbf{u} = (0, 1, 0)$). Instead of this spatial correction factor, which is of a similar form as (4), Diggle *et al.* (1995) used an isotropic correction factor, but this is only appropriate if \mathbf{X} is isotropic in the (x_1, x_2) -plane.

We prefer the translation correction factor (4), since this does not restrict the shape of W and the choice of \mathbf{u} . In a simulation study with $d = 3$, $W = [0, 1]^3$, and \mathbf{X} a Poisson line cluster point process as defined in Section 3, we obtained similar results when using the translation and the combined correction factors.

2.4 Examples

Non-parametric estimates of the cylindrical K -function for the 2D chapel data set and the 3D pyramidal cell data set are shown in Figure 3 and Figure 4, respectively. Below we comment on these plots. Further examples are given in Rafati *et al.* (2015).

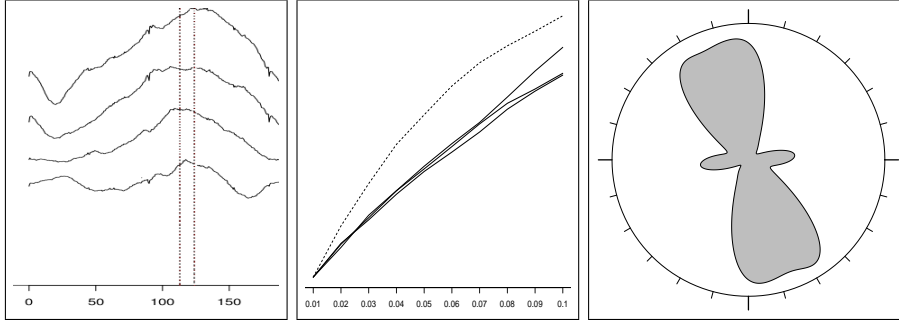


Figure 3: Chapel data set: The non-parametric estimate $\hat{K}_{(\cos \varphi, \sin \varphi)}(r, t)$ versus φ for four different combinations of r and t (left panel, with the curves from the top to the bottom corresponding to $(r, t) = (20, 40), (20, 30), (10, 30), (10, 20)$), or versus r for different values of φ and with $t = 0.3$ (middle panel, with the solid curves from the top to the bottom at $r = 0.1$ corresponding to $20^\circ, 45^\circ, 170^\circ$, and the dashed curve corresponding to $\varphi = 117^\circ$). The right panel shows a non-parametric estimate of the point pair orientation distribution function. For more details, see the text.

To detect the main direction in the chapel point pattern, the left panel in Figure 3 shows, for four different combinations of r and t , i.e. $(10, 20)$, $(10, 30)$, $(20, 30)$, and $(20, 40)$, plots of $\hat{K}_{\mathbf{u}}(r, t)$ versus φ , where $\mathbf{u} = (\cos(\varphi), \sin(\varphi))$. These four curves are approximately parallel, and a similar behaviour for other choices of r and t with $t > 2r$ was observed. In a previous analysis, Møller and Toftaker (2014) estimated the orientation of the chapel point pattern to be between 113° and 124° . This interval (specified by the dotted lines in the left panel of Figure 3) is in close agreement with the maximum of the $\hat{K}_{\mathbf{u}}(r, t)$ -curves. The middle panel in Figure 3 shows plots of $\hat{K}_{\mathbf{u}}(r, t)$ versus r when $t = 0.3$. For the dashed curve in the middle panel, $\varphi = 117^\circ$ is the average of the maximum point of φ for the four curves in the left panel, while for the three other curves in the middle panel, values of φ distinct from the interval $[113^\circ, 124^\circ]$ have been chosen. The clear difference between the dashed curve and the other curves indicates a preferred direction in the point pattern which is about 117° . This is also confirmed by the right panel in Figure 3 which shows a non-parametric estimate of the point pair orientation distribution function given by equation (14.53) in Stoyan and Stoyan (1995) and implemented in `spatstat` (Baddeley and Turner, 2005). Briefly, this is a kernel estimate which considers the direction for each pair of observed points that lie more than $r_1 = .05$ and less than $r_2 = .25$ units apart.

By the minicolumn hypothesis, the pyramidal cell data set has a columnar arrangement in the direction of the x_3 -axis shown in Figure 2 (Rafati *et al.*, 2015). Figure 4 shows that the cylindrical K -function is able to detect this kind of anisotropy: The three curves are non-parametrically estimated cylindrical functions $\hat{K}_{\mathbf{u}}(r, 80)$ for $0 < r \leq 20$ and where \mathbf{u} is parallel to one of the three main axes. The solid curve corresponding to $\mathbf{u} = (0, 0, 1)$ (i.e. when the direction of the cylinder is along the x_3 -axis) is clearly different from the two other cases where $\mathbf{u} = (1, 0, 0)$ or $\mathbf{u} = (0, 1, 0)$. The grey region is a so-called 95% simultaneous rank envelope (Myllymäki *et al.*, 2013) obtained from 999 simulated realizations under ‘complete spatial randomness’ (CSR; i.e. a stationary Poisson point process model). Roughly speaking, under CSR, each of the estimated cylindrical K -functions is expected to be within the grey region with (estimated) probability 95%. While the curves for $\mathbf{u} = (1, 0, 0)$ and $\mathbf{u} = (0, 1, 0)$ are completely within the grey region, the curve for $\mathbf{u} = (0, 0, 1)$ is clearly outside for a large range of r -values. In fact, for the null hypothesis of CSR, considering the rank envelope test (Myllymäki *et al.*, 2013) based on $\hat{K}_{\mathbf{u}}(r, 80)$ when $0 < r \leq 20$ and $\mathbf{u} = (0, 0, 1)$, the p -value is estimated to be between 0.1% and 0.18%, showing a clear deviation from the null hypothesis of CSR.

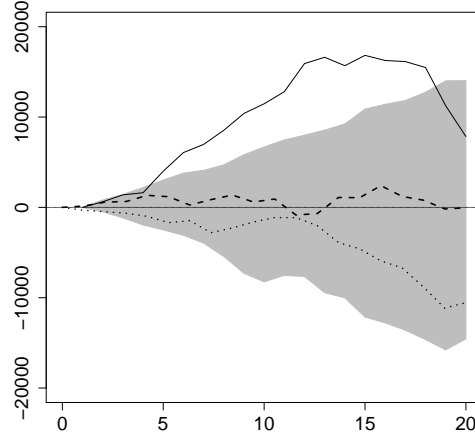


Figure 4: Pyramidal cell data set: Non-parametric estimates of the cylindrical K -function versus r when $t = 80$ and the cylinder is along the x_1 -axis (dashed line), x_2 -axis (dotted line), or x_3 -axis (solid line). The grey region specifies a 95% simultaneous rank envelope computed from 999 simulations under CSR. For more details, see the text.

These examples illustrate that the cylindrical K -function is a useful functional summary statistic for detecting preferred directions and columnar structures in a spatial point pattern.

3 The Poisson line cluster point process

This section introduces a new point process model \mathbf{X} with linear structure, by generating

- (A1) a Poisson line process $\mathbf{L} = \{l_1, l_2, \dots\}$ of (directed) lines l_i (as detailed in Section 3.1.2);
- (B1) on each line l_i , a Poisson process \mathbf{Y}_i ;
- (C1) a new point process \mathbf{X}_i obtained by random displacements in \mathbb{R}^d of the points in \mathbf{Y}_i ;
- (D1) finally, \mathbf{X} as the superposition of all the \mathbf{X}_i .

We call \mathbf{X} a *Poisson line cluster point process (PLCPP)*, since its points cluster around the Poisson lines, and we call each \mathbf{X}_i a *cluster*. Further conditions than (A1)-(D1) are specified in Section 3.1, where we also give the precise definition of a PLCPP, study the intensity and rose of directions of the Poisson line process, discuss simulation, and derive the intensity ρ and pair correlation function g for the PLCPP. Section 3.2 discusses in the special case where the lines are all parallel to a fixed direction, parameter estimation methods based on ρ and g , exploring that a Neyman-Scott process is obtained by using a certain projection. Furthermore, Section 3.3 concerns simulation-based Bayesian inference for the general case of the PLCPP model.

3.1 Definition and properties of PLCPPs

3.1.1 Notation

In addition to the notation introduced in Section 2.1, we need the following.

Denote \cdot the usual inner product on \mathbb{R}^d . For $\mathbf{u} \in \mathbb{S}^{d-1}$, let $\mathbf{u}^\perp = \{\mathbf{x} \in \mathbb{R}^d : \mathbf{x} \cdot \mathbf{u} = 0\}$ be the hyperplane perpendicular to \mathbf{u} and containing \mathbf{o} , $\lambda_{\mathbf{u}^\perp}$ the $(d-1)$ -dimensional Lebesgue measure on \mathbf{u}^\perp , and $p_{\mathbf{u}^\perp}(\mathbf{x}) = \mathbf{x} - (\mathbf{x} \cdot \mathbf{u})\mathbf{u}$ the orthogonal projection of $\mathbf{x} \in \mathbb{R}^d$ onto \mathbf{u}^\perp . Let $H = \mathbf{e}_d^\perp$ and $\lambda = \lambda_{\mathbf{e}_d^\perp}$, i.e. H is the hyperplane perpendicular to the x_d -axis.

Let k be a density function with respect to Lebesgue measure on \mathbb{R}^{d-1} . As in Section 2.1, suppose we have specified for each $\mathbf{u} \in \mathbb{S}^{d-1}$ a $d \times d$ rotation matrix $\mathcal{O}_{\mathbf{u}}$ such that $\mathbf{u} = \mathcal{O}_{\mathbf{u}}\mathbf{e}_d$. We then define a density with respect to $\lambda_{\mathbf{u}^\perp}$ by

$$k_{\mathbf{u}^\perp}(\mathcal{O}_{\mathbf{u}}(x_1, \dots, x_{d-1}, 0)) = k(x_1, \dots, x_{d-1}), \quad (x_1, \dots, x_{d-1}) \in \mathbb{R}^{d-1}.$$

In other words, when considering coordinates with respect to the $d-1$ first columns in $\mathcal{O}_{\mathbf{u}}$, the distribution under $k_{\mathbf{u}^\perp}$ is the same as under k .

3.1.2 Definition

We assume that with probability one, \mathbf{L} has no line contained in H . We use the so-called phase representation (see e.g. Chiu *et al.* (2013)), where \mathbf{L} is identified by a point process $\Phi \subset H \times \mathbb{S}^{d-1}$ such that $l = l(\mathbf{y}, \mathbf{u}) \in \mathbf{L}$ corresponds to $(\mathbf{y}, \mathbf{u}) \in H \times \mathbb{S}^{d-1}$, where \mathbf{u} is the direction of l and \mathbf{y} is the intersection point of l and H . In addition to (A1)-(D1) we assume that

- (A2) Φ is a Poisson process with intensity measure $\beta\lambda(d\mathbf{y})M(d\mathbf{u})$, where β is a positive and finite parameter and M is a probability measure on \mathbb{S}^{d-1} ;
- (B2) conditional on Φ , for each $(\mathbf{y}_i, \mathbf{u}_i) \in \Phi$, \mathbf{Y}_i is a stationary Poisson process on $l_i = l(\mathbf{y}_i, \mathbf{u}_i)$ with positive and finite intensity α , and all the \mathbf{Y}_i are independent;
- (C2) conditional on Φ , for each $(\mathbf{y}_i, \mathbf{u}_i) \in \Phi$, \mathbf{X}_i is a Poisson process on \mathbb{R}^d with intensity function

$$\Lambda_i(\mathbf{x}) = \alpha k_{\mathbf{u}_i^\perp}(p_{\mathbf{u}_i^\perp}(\mathbf{x} - \mathbf{y}_i)), \quad \mathbf{x} \in \mathbb{R}^d, \quad (5)$$

and all the \mathbf{X}_i are independent;

- (D2) in other words, the PLCPP \mathbf{X} is a Cox process with driving random intensity function $\Lambda(\mathbf{x}) = \sum_i \Lambda_i(\mathbf{x})$ for $\mathbf{x} \in \mathbb{R}^d$.

It follows from (A2) that \mathbf{L} is stationary and its distribution is given by (β, M) . By (C2), conditional on \mathbf{L} , the random displacements mentioned in (C1) are independent, and for each line $l_i = l(\mathbf{y}_i, \mathbf{u}_i) \in \mathbf{L}$ and each point $\mathbf{y}_{ij} \in \mathbf{Y}_i$, there is a corresponding point $\mathbf{x}_{ij} \in \mathbf{X}_i$ such that the random shift $\mathbf{z}_{ij} = \mathbf{x}_{ij} - \mathbf{y}_{ij}$ follows the density $k_{\mathbf{u}_i^\perp}$. We could have defined the PLCPP by letting the displacements follow a distribution on \mathbb{R}^d rather than a hyperplane, or more precisely by letting \mathbf{z}_{ij} follow a density

$$k_{\mathbf{u}_i^\perp}(p_{\mathbf{u}_i^\perp}(\mathbf{z}_{ij}))f_{\mathbf{u}_i}(\mathbf{z}_{ij} - p_{\mathbf{u}_i}(\mathbf{z}_{ij})), \quad \mathbf{z}_{ij} \in \mathbb{R}^d,$$

where $f_{\mathbf{u}_i}$ is a density function with respect to Lebesgue measure on the line $l_i - \mathbf{y}_i = \{t\mathbf{u}_i : t \in \mathbb{R}\}$. However, since the part of the displacements running along the line l_i just corresponds to independent displacements of a stationary Poisson process, this will just result in a new stationary Poisson process with the same intensity (see e.g. Section 3.3.1 in Møller and Waagepetersen (2004)), and so there is essentially no difference.

Conditional on Φ , \mathbf{X} is a Poisson process on \mathbb{R}^d with intensity function

$$\Lambda(\mathbf{x}) = \alpha \sum_{(\mathbf{y}, \mathbf{u}) \in \Phi} k_{\mathbf{u}^\perp}(p_{\mathbf{u}^\perp}(\mathbf{x} - \mathbf{y})), \quad \mathbf{x} \in \mathbb{R}^d, \quad (6)$$

cf. ((D2)). As \mathbf{L} is stationary, Λ and hence also \mathbf{X} are stationary.

Henceforth, we assume that $\int 1/|u_d| M(d\mathbf{u}) < \infty$, where u_d is the last coordinate of \mathbf{u} . The reason for making this assumption becomes clear at the end of Section 3.1.3.

3.1.2.1 Inhomogeneous case The assumption (A2) becomes important for the calculations and the statistical methodology considered later in this paper. However, to obtain a non-stationary model for \mathbf{X} , assumption (B2) may be relaxed so that α is replaced by a locally integrable function $\alpha_i = \alpha(\mathbf{y}_i, \mathbf{u}_i)$ defined on the line $l_i = l(\mathbf{y}_i, \mathbf{u}_i)$. Then (5) should be replaced by

$$\Lambda_i(\mathbf{x}) = \alpha_i((\mathbf{x} \cdot \mathbf{u}_i)\mathbf{u}_i + \mathbf{y}_i)k_{\mathbf{u}_i^\perp}(p_{\mathbf{u}_i^\perp}(\mathbf{x} - \mathbf{y}_i)), \quad \mathbf{x} \in \mathbb{R}^d,$$

and (6) by

$$\Lambda(\mathbf{x}) = \sum_{(\mathbf{y}, \mathbf{u}) \in \Phi} \alpha_{(\mathbf{y}, \mathbf{u})}((\mathbf{x} \cdot \mathbf{u})\mathbf{u} + \mathbf{y})k_{\mathbf{u}^\perp}(p_{\mathbf{u}^\perp}(\mathbf{x} - \mathbf{y})), \quad \mathbf{x} \in \mathbb{R}^d. \quad (7)$$

However this non-stationary extension of the model will be harder to analyze, e.g. moment results as established later in Section 3.1.5 for the stationary case will in general not easily extend, and it turns out that the model is not second order intensity reweighted stationary except in a special case (see Section 3.2.1.1). Moreover, while our statistical methodology in Section 3.1.5 can be straightforwardly extended, the Bayesian computations in Section 3.3 becomes harder.

3.1.3 Intensity and rose of directions for the Poisson line process

We have specified the distribution of the Poisson line process \mathbf{L} by (β, M) . This is useful for computational reasons, but when interpreting results it is usually more natural to consider the intensity and the rose of directions of \mathbf{L} , which we denote by ρ_L and \mathcal{R} , respectively. Formal definitions of these concepts are given in Appendix A, where it is shown that for any Borel set $B \subseteq \mathbb{S}^{d-1}$,

$$\rho_L = \beta \int 1/|u_d| M(d\mathbf{u}), \quad \mathcal{R}(B) = \int_B 1/|u_d| M(d\mathbf{u}) / \int 1/|u_d| M(d\mathbf{u}). \quad (8)$$

In words, ρ_L is the mean length of lines in \mathbf{L} within any region of unit volume in \mathbb{R}^d , and \mathcal{R} is the distribution of the direction of a typical line in \mathbf{L} , see e.g. Chiu *et al.* (2013).

Equation (8) establishes a one-to-one correspondence between (ρ_L, \mathcal{R}) and (β, M) , where

$$\beta = \rho_L \int |u_d| \mathcal{R}(d\mathbf{u}), \quad M(B) = \int_B |u_d| \mathcal{R}(d\mathbf{u}) / \int |u_d| \mathcal{R}(d\mathbf{u}). \quad (9)$$

Consequently, we can choose ρ_L as any positive and finite parameter, and \mathcal{R} as any probability measure on \mathbb{S}^{d-1} . Moreover, $\beta \leq \rho_L$ where the equality only holds when \mathcal{R} is concentrated with probability one at $\pm \mathbf{e}_d$. We refer to this special case as the *degenerate PLCPP*.

For the rose of directions, we later use a von Mises-Fisher distribution with concentration parameter $\kappa \geq 0$ and mean direction $\boldsymbol{\mu} \in \mathbb{S}^{d-1}$. This has a density $f(\cdot | \boldsymbol{\mu}, \kappa)$ with respect to the surface measure on \mathbb{S}^{d-1} :

$$f(\mathbf{u} | \boldsymbol{\mu}, \kappa) = c_d(\kappa) \exp(\kappa \boldsymbol{\mu} \cdot \mathbf{u}), \quad c_d(\kappa) = \frac{\kappa^{d/2-1}}{(2\pi)^{d/2} I_{d/2-1}(\kappa)}, \quad \mathbf{u} \in \mathbb{S}^{d-1}, \quad (10)$$

where I_d denotes the modified Bessel function of the first kind and order d ; in particular $c_3(\kappa) = \kappa/(4\pi \sinh \kappa)$. Note that \mathbf{L} and \mathbf{X} are then isotropic if and only if $\kappa = 0$, in which the choice of $\boldsymbol{\mu}$ plays no role. For $\kappa > 0$, the directions of the lines in \mathbf{L} are concentrated around $\boldsymbol{\mu}$, and so the clusters in \mathbf{X} have preferred direction $\boldsymbol{\mu}$. When $\boldsymbol{\mu} = \pm \mathbf{e}_d$, in the limit as $\kappa \rightarrow \infty$, we obtain the degenerate PLCPP.

3.1.4 Finite versions of the PLCPP and simulation

Suppose we want to simulate the PLCPP \mathbf{X} within a bounded region $W \subset \mathbb{R}^d$. Then we need a finite approximation of Φ (this will also be used when we later discuss Bayesian inference).

For specificity, let \mathcal{R} follow the von Mises-Fisher density $f(\mathbf{u}|\boldsymbol{\mu}, \kappa)$ and let $k(\mathbf{y}) = f(\mathbf{y}|\sigma^2)$ be the density of a $(d-1)$ -dimensional zero-mean isotropic normal density with variance σ^2 . Suppose $W_{\text{ext}} \supseteq W$ is a bounded region so that it is very unlikely that for some line $l_i = l(\mathbf{y}_i, \mathbf{u}_i) \in \mathbf{L}$ with $(\mathbf{y}_i, \mathbf{u}_i) \notin S$, \mathbf{X}_i has a point in W , where

$$S = \{(\mathbf{y}, \mathbf{u}) \in H \times \mathbb{S}^{d-1} : l(\mathbf{y}, \mathbf{u}) \cap W_{\text{ext}} \neq \emptyset\}$$

is the set of all lines hitting W_{ext} . Then our finite approximation is $\Phi_S = \Phi \cap S$.

Let ν_{d-1} denote surface measure on \mathbb{S}^{d-1} and observe that Φ_S is a Poisson process on S with intensity function

$$\chi(\mathbf{y}, \mathbf{u}|\rho_L, \boldsymbol{\mu}, \kappa) = \rho_L |u_d| f(\mathbf{u}|\boldsymbol{\mu}, \kappa)$$

with respect to the measure $\lambda(d\mathbf{y})\nu_{d-1}(d\mathbf{u})$, cf. (9). Thus the the cardinality $\#\Phi_S$ of Φ_S is Poisson distributed with mean $\rho_L I(\boldsymbol{\mu}, \kappa)$ where

$$I(\boldsymbol{\mu}, \kappa) = \int |u_d| f(\mathbf{u}|\boldsymbol{\mu}, \kappa) d\lambda(d\mathbf{y})\nu_{d-1}(d\mathbf{u}) = \int \lambda(J_{\mathbf{u}}) f(\mathbf{u}|\boldsymbol{\mu}, \kappa) \nu_{d-1}(d\mathbf{u})$$

where $J_{\mathbf{u}} = \{\mathbf{y} \in H : l(\mathbf{y}, \mathbf{u}) \cap W_{\text{ext}} \neq \emptyset\}$. Furthermore, conditional on $\#\Phi_S$, the ‘lines’ in Φ_S are i.i.d., with a density proportional to $|u_d| f(\mathbf{u}|\boldsymbol{\mu}, \kappa)$ for $\mathbf{y} \in J_{\mathbf{u}}$ (and zero otherwise). Here we use rejection sampling.

For example, if $d = 2$ and $W_{\text{ext}} = [-a, a]^2$ is a square centered at the origin, then for $\mathbf{u} = (\cos \varphi, \sin \varphi)$, we have $J_{\mathbf{u}} = J_{\varphi} \times \{0\}$ with

$$J_{\varphi} = \begin{cases} [-a \cot \varphi - a, a \cot \varphi + a] & \text{if } 0 < \varphi \leq \pi/2 \text{ or } \pi < \varphi \leq 3\pi/2, \\ [a \cot \varphi - a, a - a \cot \varphi] & \text{if } \pi/2 \leq \varphi < \pi \text{ or } 3\pi/2 \leq \varphi < 2\pi. \end{cases} \quad (11)$$

Further,

$$\lambda(J_{\mathbf{u}}) = \begin{cases} 2a + 2a \cot \varphi & \text{if } 0 < \varphi \leq \pi/2 \text{ or } \pi < \varphi \leq 3\pi/2, \\ 2a - 2a \cot \varphi & \text{if } \pi/2 \leq \varphi < \pi \text{ or } 3\pi/2 \leq \varphi < 2\pi, \end{cases} \quad (12)$$

and

$$\begin{aligned} I(\boldsymbol{\mu}, \kappa) = & 2a \int_0^{\pi/2} (\sin \varphi + \cos \varphi) f(\mathbf{u}|\boldsymbol{\mu}, \kappa) d\varphi + 2a \int_{\pi/2}^{\pi} (\sin \varphi - \cos \varphi) f(\mathbf{u}|\boldsymbol{\mu}, \kappa) d\varphi \\ & - 2a \int_{\pi}^{3\pi/2} (\sin \varphi + \cos \varphi) f(\mathbf{u}|\boldsymbol{\mu}, \kappa) d\varphi - 2a \int_{3\pi/2}^{2\pi} (\sin \varphi - \cos \varphi) f(\mathbf{u}|\boldsymbol{\mu}, \kappa) d\varphi, \end{aligned} \quad (13)$$

which can be evaluated by numerical methods. Furthermore, for $\boldsymbol{\mu} = (\cos \theta, \sin \theta)$ and $\mathbf{y} = (y_1, y_2)$, the unnormalized density $|u_d| f(\mathbf{u}|\boldsymbol{\mu}, \kappa) = \mathbf{1}[y_1 \in J_{\varphi}] |\sin \varphi| \exp(\kappa \cos(\varphi - \theta))$ is just with respect to Lebesgue measure $dy_1 d\varphi$ on $\mathbb{R} \times [0, 2\pi)$. Finally, when doing rejection sampling, we propose φ from $f(\cdot|\boldsymbol{\mu}, \kappa)$ and y_1 from the uniform distribution on J_{φ} , and accept (φ, y_1) with probability $|\sin \varphi|$.

3.1.5 Moments

Since the PLCPP \mathbf{X} is a Cox process with driving random intensity Λ , \mathbf{X} has intensity ρ and pair correlation function g given by

$$\rho = \mathbb{E}[\Lambda(\mathbf{o})], \quad \rho^2 g(\mathbf{x}) = \mathbb{E}[\Lambda(\mathbf{o})\Lambda(\mathbf{x})], \quad \mathbf{x} \in \mathbb{R}^d. \quad (14)$$

Appendix B verifies that

$$\rho = \alpha \rho_L \quad (15)$$

and

$$g(\mathbf{x}) = 1 + \frac{1}{\rho_L} \int k_{\mathbf{u}^\perp} * \tilde{k}_{\mathbf{u}^\perp}(p_{\mathbf{u}^\perp}(\mathbf{x})) \mathcal{R}(\mathrm{d}\mathbf{u}), \quad \mathbf{x} \in \mathbb{R}^d, \quad (16)$$

where $\tilde{k}_{\mathbf{u}^\perp}(p_{\mathbf{u}^\perp}(\mathbf{x})) = k_{\mathbf{u}^\perp}(-p_{\mathbf{u}^\perp}(\mathbf{x}))$ and $*$ denotes convolution, i.e.

$$k_{\mathbf{u}^\perp} * \tilde{k}_{\mathbf{u}^\perp}(p_{\mathbf{u}^\perp}(\mathbf{x})) = \int k_{\mathbf{u}^\perp}(p_{\mathbf{u}^\perp}(\mathbf{x}) - \mathbf{y}) \tilde{k}_{\mathbf{u}^\perp}(\mathbf{y}) \lambda_{\mathbf{u}^\perp}(\mathrm{d}\mathbf{y}).$$

Thus $g > 1$, reflecting the clustering of the PLPCP. Evaluation of the integral in (16) may require numerical methods. For example, if $k(\cdot) = f(\cdot|\sigma^2)$ (the density of the $(d-1)$ -dimensional zero-mean isotropic normal distribution with variance $\sigma^2 > 0$), then

$$k_{\mathbf{u}^\perp} * \tilde{k}_{\mathbf{u}^\perp}(p_{\mathbf{u}^\perp}(\mathbf{x})) = \exp(-\|p_{\mathbf{u}^\perp}(\mathbf{x})\|^2 / (4\sigma^2)) / (4\pi\sigma^2). \quad (17)$$

3.2 Moment based inference

The likelihood for a parametric PLCPP model is complicated because of the hidden line process and the hidden point processes on the lines, though it can be approximated using a missing data Markov chain Monte Carlo (MCMC) approach (see e.g. Møller and Waagepetersen (2004)); such an approach is used in Section 3.3 but in a Bayesian context. Simpler procedures for parameter estimation are composite likelihood (Guan, 2006; Møller and Waagepetersen, 2007) and minimum contrast methods (Diggle and Gratton, 1984) based on (15)-(16). Since g is hard to compute in general, this section focuses on such procedures in the special case of a degenerate PLCPP which e.g. could be a relevant model for the pyramidal cell data set (Figure 2). For specificity we assume as in (17) that $k(\cdot) = f(\cdot|\sigma^2)$. Then the unknown parameters are $\beta = \rho_L > 0$, $\alpha > 0$, and $\sigma^2 > 0$.

3.2.1 Projections

Assume that a realization of $\mathbf{X}_W = \mathbf{X} \cap W$ is observed within a region of the product form $W = D \times I$, where $D \subset \mathbb{R}^{d-1}$ and $I \subset \mathbb{R}$ are bounded sets. Denote \mathbf{X}_I the projection of $\mathbf{X} \cap (\mathbb{R}^{d-1} \times I)$ onto I . Then \mathbf{X}_I is a sufficient statistic, since the x_d -coordinates of the points in \mathbf{X}_W are i.i.d. uniform points on I which are independent of \mathbf{X}_I .

Note that \mathbf{X}_I is a Neyman-Scott process or more precisely a modified Thomas process (Neyman and Scott, 1958; Møller and Waagepetersen, 2004), i.e. a Cox process driven by the random intensity function

$$\Gamma(\mathbf{x}) = \alpha |I| \sum_i f(\mathbf{x} - \mathbf{y}_i | \sigma^2), \quad \mathbf{x} \in H,$$

where the \mathbf{y}_i s are coming from Φ and constitute a stationary Poisson process on H with intensity ρ_L . The modified Thomas process has intensity $\rho_I = \rho |I|$ and pair correlation function

$$g_I(\mathbf{x}) = 1 + \frac{1}{(4\pi\sigma^2)^{d/2} \rho_L} \exp\left(-\frac{\|\mathbf{x}\|^2}{4\sigma^2}\right), \quad \mathbf{x} \in H,$$

in agreement with (16).

Parameter estimation based on (ρ_I, g_I) and using a composite likelihood or a minimum contrast method is straightforward (Møller and Waagepetersen, 2007). Then, when checking a fitted Thomas process, we should not reuse the intensity and the pair correlation function. Below we use instead the functional summary statistics F (the empty space function), G (the nearest-neighbour function), and the J -function (see e.g. Møller and Waagepetersen (2004)).

3.2.1.1 Inhomogeneous case Consider the inhomogeneous case where \mathbf{X} is a Cox process with driving random intensity function (7), assuming that the intensity function $\alpha(\mathbf{y}, \mathbf{e}_d)(y_1, \dots, y_{d-1}, x_d) = \alpha(x_d)$ does not depend on $\mathbf{y} = (y_1, \dots, y_{d-1}, 0) \in H$. Let $c = \int_I \alpha$. Then it can be shown that \mathbf{X} is second order intensity reweighted stationary, \mathbf{X}_I is still a Neyman-Scott process as above, while the x_d -coordinates of the points in \mathbf{X}_W are i.i.d. with density α/c , and they are independent of \mathbf{X}_W . Moreover, statistical inference simply splits into modelling the density α/c based on the x_d -coordinates of the points in \mathbf{X}_W and inferring (c, ρ_L, σ^2) by considering \mathbf{X}_I along similar lines as above but with $\alpha|I|$ replaced by c .

3.2.2 Example

In accordance with the minicolumn hypothesis, we assume that the 3D pyramidal cell data set in Figure 2 has a columnar arrangement in the direction of the x_3 -axis. Then, assuming a PLCPP model it should be a degenerate PLCPP. Further, the observation window is of the same form as in Section 3.2.1, with $D = [0, 508] \times [0, 138]$ and $I = [0, 320]$. The first panel in Figure 5 shows a histogram of the x_3 -coordinates of the pyramidal cell point pattern data set, and there is no clear indication of a deviation from a uniform distribution.

When fitting the modified Thomas process for the projected point pattern onto D , for both composite likelihood and minimum contrast estimation, we used the `spatstat` (Baddeley and Turner, 2005) function `kppm`. We obtained the minimum contrast estimates $\hat{\rho}_L = 0.024$, $\hat{\alpha} = 0.37/320 = 0.0012$, and $\hat{\sigma}^2 = 15.04$, and similar estimates were obtained using the composite likelihood method. The three last panels in Figure 5 show the non-parametric estimated F , G , and J -functions for the projected pyramidal cell point pattern onto D (solid lines), together with 95% simultaneous rank envelopes (gray regions) obtained using 4999 simulated point patterns under the fitted Thomas process. The p -values for the rank envelope test (Myllymäki *et al.*, 2013) for G , F , and J -functions are, respectively, within the intervals $[0.851, 0.852]$, $[0.732, 0.733]$, and $[0.623, 0.625]$, providing no evidence against the fitted model (Myllymäki *et al.* (2013) recommended 4999 simulations for F, G, J ; however, for the cylindrical K -function considered in Figure 4, 999 simulations seemed sufficient).

3.3 Bayesian inference

Suppose we model \mathbf{X} as a PLCPP and a non-empty realization $\mathbf{X}_W = \{\mathbf{x}_1, \dots, \mathbf{x}_n\}$ is our data, where $W \subset \mathbb{R}^d$ is a bounded observation window. For specificity and clarity, let $k_{\mathbf{u}^\perp}(\mathbf{y}) = f(\mathbf{y}|\sigma^2)$ and let \mathcal{R} follow the von Mises-Fisher density $f(\mathbf{u}|\boldsymbol{\mu}, \kappa)$ given by (10). Moreover, as in Section 3.1.4, we approximate the hidden process Φ by the finite version Φ_S . This section considers a missing data MCMC approach for Bayesian inference concerning Φ_S (the ‘missing data’) and the parameters $\rho_L > 0$, $\boldsymbol{\mu} \in \mathbb{S}^{d-1}$, $\kappa > 0$, $\alpha > 0$, $\sigma^2 > 0$.

3.3.1 Posterior specification and simulation-based approach

Using the approximation Φ_S of Φ , we consider \mathbf{X}_W as a finite Cox process with driving random intensity function

$$\Lambda(\mathbf{x}|\Phi_S, \alpha, \sigma^2) = \alpha \sum_{(\mathbf{y}, \mathbf{u}) \in \Phi_S} f(p_{\mathbf{u}^\perp}(\mathbf{x} - \mathbf{y})|\sigma^2).$$

Then conditional on Φ_S , \mathbf{X}_W is absolutely continuous with respect to the unit rate Poisson process on W , with density

$$f(\{\mathbf{x}_1, \dots, \mathbf{x}_n\}|\Phi_S, \alpha, \sigma^2) = \exp\left(|W| - \int_W \Lambda(\mathbf{x}|\Phi_S, \alpha, \sigma^2) d\mathbf{x}\right) \prod_{i=1}^n \Lambda(\mathbf{x}_i|\Phi_S, \alpha, \sigma^2) \quad (18)$$

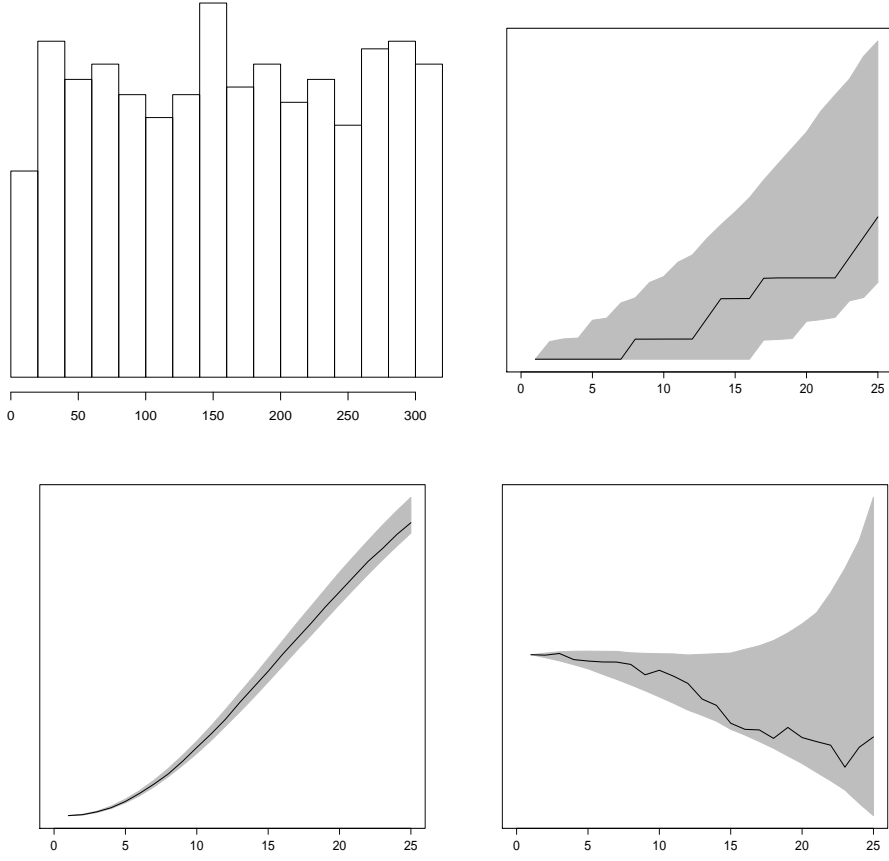


Figure 5: Histogram of the x_3 -coordinates of the pyramidal cell point pattern data set (top left), and non-parametric estimates of G (top right), F (bottom left), and J (bottom right) for the projected pyramidal cell point pattern onto D (solid lines), together with 95% simultaneous rank envelopes (gray regions) obtained using 4999 simulated point patterns under the fitted Thomas process.

for finite point configurations $\{\mathbf{x}_1, \dots, \mathbf{x}_n\} \subset W$.

The distribution of Φ_S is absolutely continuous with respect to the distribution of a natural reference process $\Phi_{0,S}$ defined as the Poisson process on S with intensity function $\chi_0(\mathbf{y}, \mathbf{u}) = |u_d| \Gamma(d/2) / (2\pi^{d/2})$ (with respect to the measure $\lambda(d\mathbf{y})\nu_{d-1}(d\mathbf{u})$, cf. Section 3.1.4). This reference process corresponds to the case of an isotropic Poisson line process with unit intensity. The density of Φ_S with respect to the distribution of $\Phi_{0,S}$ is

$$\begin{aligned} & f(\{(\mathbf{y}_1, \mathbf{u}_1), \dots, (\mathbf{y}_k, \mathbf{u}_k)\} | \rho_L, \boldsymbol{\mu}, \kappa) \\ &= \exp \left(\int_S [\chi_0(\mathbf{y}, \mathbf{u}) - \chi(\mathbf{y}, \mathbf{u} | \rho_L, \boldsymbol{\mu}, \kappa)] \lambda(d\mathbf{y})\nu_{d-1}(d\mathbf{u}) \right) \prod_{j=1}^k \frac{\chi(\mathbf{y}_j, \mathbf{u}_j | \rho_L, \boldsymbol{\mu}, \kappa)}{\chi_0(\mathbf{y}_j, \mathbf{u}_j)} \end{aligned}$$

for finite point configurations $\{(\mathbf{y}_1, \mathbf{u}_1), \dots, (\mathbf{y}_k, \mathbf{u}_k)\} \subset S$. That is, using the notation in Section 3.1.4,

$$\begin{aligned} & f(\{(\mathbf{y}_1, \mathbf{u}_1), \dots, (\mathbf{y}_k, \mathbf{u}_k)\} | \rho_L, \boldsymbol{\mu}, \kappa) \\ & \propto \exp(-\rho_L I(\boldsymbol{\mu}, \kappa)) \prod_{j=1}^k \left[\frac{2\pi^{d/2}}{\Gamma(d/2)} \rho_L f(\mathbf{u}_j | \boldsymbol{\mu}, \kappa) \mathbf{1}[\mathbf{y}_j \in J_{\mathbf{u}_j}] \right], \end{aligned} \quad (19)$$

where we have omitted a constant not depending on the parameters.

Imaging that also a realization $\Phi_S = \{(\mathbf{y}_1, \mathbf{u}_1), \dots, (\mathbf{y}_k, \mathbf{u}_k)\}$ had been observed, the likelihood becomes

$$\begin{aligned} & l(\alpha, \sigma^2, \rho_L, \boldsymbol{\mu}, \{(\mathbf{y}_1, \mathbf{u}_1), \dots, (\mathbf{y}_k, \mathbf{u}_k)\}) \\ &= f(\{\mathbf{x}_1, \dots, \mathbf{x}_n\} | \{(\mathbf{y}_1, \mathbf{u}_1), \dots, (\mathbf{y}_k, \mathbf{u}_k)\}, \alpha, \sigma^2) f(\{(\mathbf{y}_1, \mathbf{u}_1), \dots, (\mathbf{y}_k, \mathbf{u}_k)\} | \rho_L, \boldsymbol{\mu}, \kappa). \end{aligned} \quad (20)$$

Imposing independent prior densities $p(\rho_L), p(\boldsymbol{\mu}), p(\kappa), p(\alpha), p(\sigma^2)$ on the parameters, we obtain the posterior density

$$\begin{aligned} & p(\rho_L, \boldsymbol{\mu}, \kappa, \alpha, \sigma^2, \{(\mathbf{y}_1, \mathbf{u}_1), \dots, (\mathbf{y}_k, \mathbf{u}_k)\} | \{\mathbf{x}_1, \dots, \mathbf{x}_n\}) \\ & \propto l(\rho_L, \boldsymbol{\mu}, \kappa, \alpha, \sigma^2 | \{\mathbf{x}_1, \dots, \mathbf{x}_n\}, \{(\mathbf{y}_1, \mathbf{u}_1), \dots, (\mathbf{y}_k, \mathbf{u}_k)\}) p(\rho_L) p(\boldsymbol{\mu}) p(\kappa) p(\alpha) p(\sigma^2). \end{aligned} \quad (21)$$

Further prior specifications are given in our example in Section 3.3.2. Since the posterior is analytically intractable, a hybrid MCMC algorithm (or Metropolis within Gibbs algorithm, see e.g. Gilks, Richardson and Spiegelhalter (1996)) is proposed in Appendix C. Briefly, the algorithm alternates between updating each of the parameters and the line process, using a birth-death-move Metropolis-Hastings algorithm for the line process.

3.3.2 Example

We illustrate the Bayesian approach using the 2D chapel data set in Figure 2.

The observation window $W = [-.5, .5]^2$ is a unit square which we let be centered around the origin. Based on experimentation the value $a = 0.55$ for $W_{\text{ext}} = [-a, a]^2$ seemed large enough to account for edge effects. For the hybrid MCMC algorithm we used 200,000 iterations (one iteration consists of updating all the parameters and the missing data). We considered trace plots (omitted here) for the parameters and information about the missing data, indicating that a burn-in of 5000 iterations is sufficient.

We used a uniform prior for both $\boldsymbol{\mu} = (\cos \varphi, \sin \varphi)$ and σ^2 , and flat conjugated gamma priors for ρ_L and α , see Figure 6. Our posterior results for ρ_L , φ , and α were sensitive to the choice of prior distribution for κ . For small values of κ (< 30), meaningless posterior results appeared, since φ was approximately uniform, and for φ close to zero, ρ_L tended

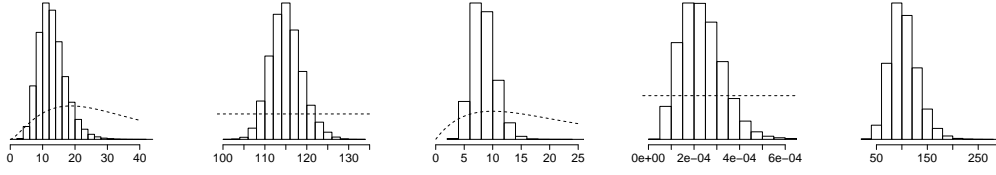


Figure 6: The first four panels show the unnormalized prior density (dashed line) and histogram for the posterior distribution of ρ_L , φ , α , and σ^2 , respectively. The final panel shows the histogram for the posterior distribution of ρ .

to zero (and hence α to infinity). On the other hand, very large values of κ cause a very concentrated posterior distribution for φ . As a compromise, after some experimentation, we fixed $\kappa = 40$ (admitting that this is a kind of empirical Bayesian approach).

There is a clear distinction between the simulated posterior results for the parameters and the priors, cf. the first four panels in Figure 6. In fact these posterior results were not so sensitive to other prior specifications of ρ_L , φ , α , and σ^2 . Note that the posterior mean of φ (115.02°) is in close agreement with the result of 117° found in Section 2.4, and σ is unlikely to be larger than 0.02 (indicating that the points are rather close to the lines and that the choice $a = 0.55$ makes sense). The final panel in Figure 6 shows a good agreement between the number of chapels (110) and the posterior mean of the intensity ρ (103.7), though there is some uncertainty in the posterior distribution of ρ . Moreover, the posterior means of ρ_L and α are 12.9 and 8.4, respectively, which combined with (15) result in the estimate 108.4 for ρ .

To illustrate the usefulness of the Bayesian method in detecting linear structures, Figure 7 shows a posterior kernel estimate of the density of lines within W . The estimate visualizes where the hidden lines could be (the lighter areas), and overall they agree with the point pattern of chapels (superimposed in the figure) though in the upper right corner of the observation window there is some ‘doubt’ about whether there should be a single or two clusters of points. Specifically, the estimate is obtained from 100 posterior iterations with an equal spacing, and it is the average of binary pixel representations of the line process, where a pixel has value 1 if it is intersected by a line, and value 0 otherwise.

Acknowledgments

Supported by the Danish Council for Independent Research | Natural Sciences, grant 12-124675, "Mathematical and Statistical Analysis of Spatial Data", and by the "Centre for Stochastic Geometry and Advanced Bioimaging", funded by grant 8721 from the Villum Foundation. We thank Jens Randel Nyengaard, Karl-Anton Dorph-Petersen, and Ali H. Rafati for collecting the 3D pyramidal cell data set.

Appendix A: Intensity and rose of direction

Let $|\cdot|_1$ denote one-dimensional Lebesgue measure, dt Lebesgue measure on the real line, and $A \subseteq \mathbb{R}^d$ and $B \subseteq \mathbb{S}^{d-1}$ arbitrary Borel sets.

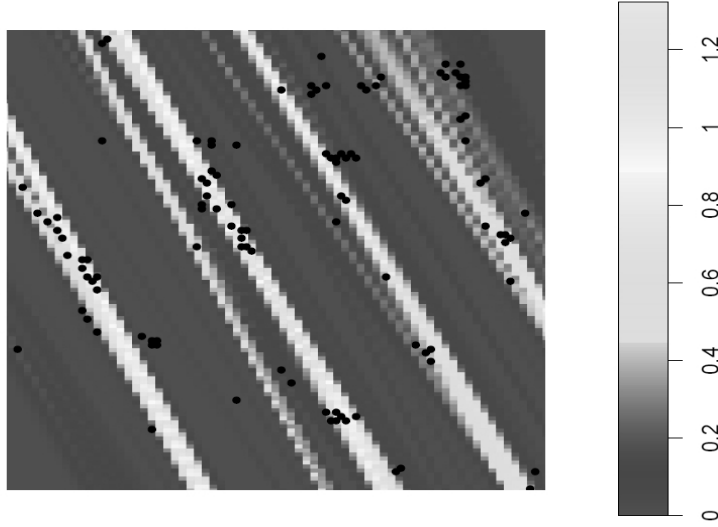


Figure 7: Posterior kernel estimate of the density of lines. For comparison, the chapel point pattern data set is superimposed.

By definition of the intensity, for an arbitrary Borel set $A \subseteq \mathbb{R}^d$ with volume $|A|$,

$$\rho_L |A| = \mathbb{E} \sum_{l \in \mathbf{L}} |l \cap A|_1$$

where $|\cdot|_1$ denotes one-dimensional Lebesgue measure and dt Lebesgue measure on the real line. Further, by definition of the rose of directions, for an arbitrary Borel set $B \subseteq \mathbb{S}^{d-1}$,

$$\rho_L |A| \mathcal{R}(B) = \mathbb{E} \sum_{l \in \mathbf{L}} |l \cap A|_1 1[\mathbf{u} \in B]. \quad (22)$$

The right hand side in (22) equals

$$\mathbb{E} \sum_{(\mathbf{y}, \mathbf{u}) \in \Phi} \int 1[\mathbf{y} + t\mathbf{u} \in A, \mathbf{u} \in B] dt \quad (23)$$

$$= \beta \int \int \int 1[\mathbf{y} + t\mathbf{u} \in A, \mathbf{u} \in B] dt \lambda(d\mathbf{y}) M(d\mathbf{u}) \quad (24)$$

$$= \beta |A| \int_B 1/|u_d| M(d\mathbf{u}) \quad (25)$$

whereby (8) is verified. Here (23) follows from the phase representation of \mathbf{L} (see Section 3.1.2), (24) from the Slivnyak-Mecke theorem for the Poisson process Φ (see e.g. Møller and Waagepetersen (2004)), and (25) since $|u_d|$ is the Jacobian of the mapping $(t, \mathbf{y}) \mapsto \mathbf{y} + t\mathbf{u}$ with $(t, \mathbf{y}) \in \mathbb{R} \times H$. Note that (8) and $0 < \beta < \infty$ imply that $0 < \rho_L < \infty$. Hence by (22) and stationarity of \mathbf{L} , \mathcal{R} is a probability measure.

Appendix B: Moments

It remains to verify (15)-(16).

Proof of (15): By (6), (14), and the Slivnyak-Mecke theorem for the Poisson process,

$$\rho = \alpha \beta \int \int k_{\mathbf{u}}(-p_{\mathbf{u}}(\mathbf{y})) \lambda(d\mathbf{y}) M(d\mathbf{u}). \quad (26)$$

Let I_d be the $d \times d$ identity matrix, and \mathbf{o}_{d-1} the origin in \mathbb{R}^{d-1} . For $\mathbf{u} \in \mathbb{S}^{d-1}$, let $A(\mathbf{u}) = \mathbf{v}\mathbf{v}^T$ where \mathbf{v} is the subvector consisting of the first $d-1$ coordinates of \mathbf{u} and T denotes transposition. The Jacobian of the linear transformation

$$p_{\mathbf{u}}(\mathbf{y}) = [I_d - \mathbf{u}\mathbf{u}^T] \mathbf{y}, \quad \mathbf{y} \in H,$$

is the square root of the determinant of the $(d-1) \times (d-1)$ matrix

$$\begin{aligned} Q &= \left[[I_d - \mathbf{u}\mathbf{u}^T] [I_{d-1} \ \mathbf{o}_{d-1}]^T \right]^T [I_d - \mathbf{u}\mathbf{u}^T] [I_{d-1} \ \mathbf{o}_{d-1}]^T \\ &= [I_{d-1} \ \mathbf{o}_{d-1}] [I_d - \mathbf{u}\mathbf{u}^T] [I_{d-1} \ \mathbf{o}_{d-1}]^T \\ &= I_{d-1} - A(\mathbf{u}). \end{aligned}$$

Since $A(\mathbf{u})$ is symmetric of rank at most one and has trace $\text{tr}(A(\mathbf{u})) = u_1^2 + \dots + u_{d-1}^2 = 1 - u_d^2$, the determinant of Q is $1 - \text{tr}(A(\mathbf{u})) = u_d^2$. Combining this with (26) we obtain

$$\rho = \alpha\beta \int \int k_{\mathbf{u}}(-\mathbf{y})/|u_d| \lambda_{\mathbf{u}}(d\mathbf{y}) M(d\mathbf{u}).$$

Thereby (15) easily follows from the first identity in (8).

Proof of (16): By (6) and (14),

$$\begin{aligned} \rho^2 g(\mathbf{x}) &= \alpha^2 \mathbb{E} \sum_{i \neq j} k_{\mathbf{u}_i^+}(p_{\mathbf{u}_i^+}(-\mathbf{y}_i)) k_{\mathbf{u}_j^+}(p_{\mathbf{u}_j^+}(\mathbf{x} - \mathbf{y}_j)) \\ &\quad + \alpha^2 \mathbb{E} \sum_i k_{\mathbf{u}_i^+}(p_{\mathbf{u}_i^+}(-\mathbf{y}_i)) k_{\mathbf{u}_i^+}(p_{\mathbf{u}_i^+}(\mathbf{x} - \mathbf{y}_i)) \\ &= \rho^2 + \alpha^2 \beta \int k_{\mathbf{u}^+}(p_{\mathbf{u}^+}(-\mathbf{y})) k_{\mathbf{u}^+}(p_{\mathbf{u}^+}(\mathbf{x} - \mathbf{y})) \lambda(d\mathbf{y}) M(d\mathbf{u}) \end{aligned} \quad (27)$$

using the extended Slivnyak-Mecke theorem for the Poisson process and the proof of (15) to obtain that the first expectation is equal to ρ^2 , and the Slivnyak-Mecke theorem for the Poisson process to obtain that the second expectation is equal to the last term. Combining (15) and (27) with the result for the Jacobian considered above, we obtain (16).

Appendix C: Hybrid MCMC algorithm

This appendix gives the details for the hybrid MCMC algorithm considered in Section 3.3.1.

Recall that $p(\rho_L), p(\boldsymbol{\mu}), p(\kappa), p(\alpha), p(\sigma^2)$ are the independent prior densities. As in Section 3.3.2, for α and ρ_L we consider conjugated gamma priors; denote their shape parameters by a_1 and a_2 and their inverse scale parameters by b_1 and b_2 , respectively. For the remaining parameters, we just consider generic prior densities, since they have no (well-known) conjugate priors, cf. (18) and (19).

Suppose $(\rho_L, \boldsymbol{\mu}, \kappa, \alpha, \sigma^2, \{(\mathbf{y}_1, \mathbf{u}_1), \dots, (\mathbf{y}_k, \mathbf{u}_k)\})$ is the current state of the hybrid MCMC algorithm, where $n \geq 1$, $k \geq 1$ (since $k = 0$ implies $n = 0$, which is not a case of interest), and $l(\mathbf{y}_i, \mathbf{u}_i) \cap W_{\text{ext}} \neq \emptyset, i = 1, \dots, k$. Combining (18)-(21) we notice the following, when we are either updating one of the parameters or the missing data (in the case of Section 3.3.2 where the value of κ is fixed, we can of course just ignore the update of κ described below).

We use a Gibbs update for α respective ρ_L , noting that the conditional distribution of α given the rest is a gamma distribution with shape parameter $a_1 + n$ and inverse scale parameter $b_1 + \int_W \sum_{j=1}^k f(p_{\mathbf{u}_j^+}(\mathbf{x} - \mathbf{y}_j) | \sigma^2) d\mathbf{x}$, and the conditional distribution of ρ_L given the rest is a gamma distribution with shape parameter $a_2 + k$ and inverse scale parameter $b_2 + I(\boldsymbol{\mu}, \kappa)$.

For the remaining parameters $\boldsymbol{\mu}$, κ , and σ^2 , we use Metropolis random walk updates, with a von Mises-Fisher proposal for $\boldsymbol{\mu}$ and normal proposals for κ and σ^2 which are tuned such that the mean acceptance probabilities are between 20-45% (as recommended in Roberts, Gelman and Gilks (1997)). When proposing updating $\boldsymbol{\mu}$ by $\boldsymbol{\mu}'$, and κ by κ' , the Hastings ratios simply become

$$R_{\boldsymbol{\mu}} = \frac{p(\boldsymbol{\mu}')}{p(\boldsymbol{\mu})} \exp(\rho_L [I(\boldsymbol{\mu}, \kappa) - I(\boldsymbol{\mu}', \kappa)]) \prod_{j=1}^k \frac{f(\mathbf{u}_j | \boldsymbol{\mu}', \kappa)}{f(\mathbf{u}_j | \boldsymbol{\mu}, \kappa)}$$

and

$$R_{\kappa} = \frac{p(\kappa')}{p(\kappa)} \exp(\rho_L [I(\boldsymbol{\mu}, \kappa) - I(\boldsymbol{\mu}, \kappa')]) \prod_{j=1}^k \frac{f(\mathbf{u}_j | \boldsymbol{\mu}, \kappa')}{f(\mathbf{u}_j | \boldsymbol{\mu}, \kappa)}.$$

However, when updating σ^2 by a proposal σ'^2 , the Hastings ratio becomes

$$R_{\sigma^2} = \frac{p(\sigma'^2)}{p(\sigma^2)} \exp \left(\alpha \sum_{j=1}^k \left[\int_W f(p_{\mathbf{u}_j^\perp}(\mathbf{x} - \mathbf{y}_j) | \sigma^2) d\mathbf{x} - \int_W f(p_{\mathbf{u}_j^\perp}(\mathbf{x} - \mathbf{y}_j) | \sigma'^2) d\mathbf{x} \right] \right) \\ \times \prod_{i=1}^n \frac{\sum_{j=1}^k f(p_{\mathbf{u}_j^\perp}(\mathbf{x}_i - \mathbf{y}_j) | \sigma'^2)}{\sum_{j=1}^k f(p_{\mathbf{u}_j^\perp}(\mathbf{x}_i - \mathbf{y}_j) | \sigma^2)}$$

where each integral is calculated by a simple Monte Carlo method after making a change of variables from \mathbf{x} to its Cartesian coordinates in a system centered at \mathbf{y}_j and with axes given by \mathbf{u}_j and \mathbf{u}_j^\perp .

For the missing data, we use the birth-death-move Metropolis-Hastings algorithm in Geyer and Møller (1994) as follows. The proposal probability for each of the birth/death/move type proposals happens with probability 1/3. If a birth is proposed, the proposal consists of adding a new point (\mathbf{y}, \mathbf{u}) , where $\mathbf{u} \sim f(\cdot | \boldsymbol{\mu}, \kappa)$ and \mathbf{y} conditional on \mathbf{u} is uniformly distributed on $J_{\mathbf{u}}$, and (as explained below) the Hastings ratio becomes

$$R_{\text{birth}} = \frac{\rho_L \lambda(J_{\mathbf{u}}) |u_d|}{k+1} \mathbf{1}[l(\mathbf{y}, \mathbf{u}) \cap W_{\text{ext}} \neq \emptyset] \\ \times \exp \left(-\alpha \int_W f(p_{\mathbf{u}^\perp}(\mathbf{x} - \mathbf{y}) | \sigma^2) d\mathbf{x} \right) \prod_{i=1}^n \left(1 + \frac{f(p_{\mathbf{u}^\perp}(\mathbf{x}_i - \mathbf{y}) | \sigma^2)}{\sum_{j=1}^k f(p_{\mathbf{u}_j^\perp}(\mathbf{x}_i - \mathbf{y}_j) | \sigma^2)} \right). \quad (28)$$

To stress the dependence on $\{(\mathbf{y}_1, \mathbf{u}_1), \dots, (\mathbf{y}_k, \mathbf{u}_k)\}$ and (\mathbf{y}, \mathbf{u}) , we write

$$R_{\text{birth}} = R_{\text{birth}}(\mathbf{y}_1, \mathbf{u}_1, \dots, \mathbf{y}_k, \mathbf{u}_k; \mathbf{y}, \mathbf{u})$$

(obviously, it also depends on ρ_L, α, σ^2 , and $\{\mathbf{x}_1, \dots, \mathbf{x}_n\}$). If a death is proposed, we generate a uniform $j \in \{1, \dots, k\}$ (provided $k > 1$; if $k = 1$, we do nothing and keep the current state) and propose to delete $(\mathbf{y}_j, \mathbf{u}_j)$, and (as explained below) the Hastings ratio is

$$R_{\text{death}} = 1/R_{\text{birth}}(\mathbf{y}_1, \mathbf{u}_1, \dots, \mathbf{y}_{j-1}, \mathbf{u}_{j-1}, \mathbf{y}_{j+1}, \mathbf{u}_{j+1}, \dots, \mathbf{y}_k, \mathbf{u}_k; \mathbf{y}_j, \mathbf{u}_j). \quad (29)$$

If a move is proposed, then we select a uniform $j \in \{1, \dots, k\}$ and propose to replace $(\mathbf{y}_j, \mathbf{u}_j)$ by $(\mathbf{y}'_j, \mathbf{u}'_j)$, where $\mathbf{u}'_j \sim f(\cdot | \boldsymbol{\mu}, \kappa)$ and \mathbf{y}'_j conditional on \mathbf{u}'_j is uniformly distributed on $J_{\mathbf{u}'_j}$; since this can be considered as first a death proposal and second a birth proposal, the Hastings ratio is

$$R_{\text{move}} = \frac{R_{\text{birth}}(\mathbf{y}_1, \mathbf{u}_1, \dots, \mathbf{y}_{j-1}, \mathbf{u}_{j-1}, \mathbf{y}_{j+1}, \mathbf{u}_{j+1}, \dots, \mathbf{y}_k, \mathbf{u}_k; \mathbf{y}'_j, \mathbf{u}'_j)}{R_{\text{birth}}(\mathbf{y}_1, \mathbf{u}_1, \dots, \mathbf{y}_{j-1}, \mathbf{u}_{j-1}, \mathbf{y}_{j+1}, \mathbf{u}_{j+1}, \dots, \mathbf{y}_k, \mathbf{u}_k; \mathbf{y}_j, \mathbf{u}_j)}.$$

Finally, for each type of updates, the proposal is accepted with probability $\min\{1, R\}$, where R is the corresponding Hastings ratio.

It remains to explain how we obtain the Hastings ratios (28)-(29). Recall that the reference Poisson process $\Phi_{0,S}$ has intensity measure

$$\zeta(d\mathbf{y}, d\mathbf{u}) = |u_d| \frac{\Gamma(d/2)}{2\pi^{d/2}} \lambda(d\mathbf{y}) \nu_{d-1}(d\mathbf{u}).$$

Further, conditional on the data $\mathbf{X}_W = \{\mathbf{x}_1, \dots, \mathbf{x}_n\}$ and the parameters $\rho_L, \boldsymbol{\mu}, \kappa, \alpha, \sigma^2$, the target process Φ_S has density

$$\begin{aligned} & f(\{(\mathbf{y}_1, \mathbf{u}_1), \dots, (\mathbf{y}_k, \mathbf{u}_k)\} | \{\mathbf{x}_1, \dots, \mathbf{x}_n\}, \alpha, \sigma^2, \rho_L, \boldsymbol{\mu}, \kappa) \\ & \propto f(\{\mathbf{x}_1, \dots, \mathbf{x}_n\} | \{(\mathbf{y}_1, \mathbf{u}_1), \dots, (\mathbf{y}_k, \mathbf{u}_k)\}, \alpha, \sigma^2) f(\{(\mathbf{y}_1, \mathbf{u}_1), \dots, (\mathbf{y}_k, \mathbf{u}_k)\} | \rho_L, \boldsymbol{\mu}, \kappa) \end{aligned}$$

with respect to the distribution of $\Phi_{0,S}$. Furthermore, if a birth (\mathbf{y}, \mathbf{u}) is proposed, then it has density

$$f(\mathbf{y}, \mathbf{u} | \boldsymbol{\mu}, \kappa) = \frac{f(\mathbf{u} | \boldsymbol{\mu}, \kappa) \mathbf{1}[\mathbf{y} \in J_{\mathbf{u}}] / \lambda(J_{\mathbf{u}})}{|u_d| \Gamma(d/2) / (2\pi^{d/2})}$$

with respect to ζ . Consequently, by Geyer and Møller (1994), the Hastings ratio for the proposed birth is

$$\begin{aligned} R_{\text{birth}} &= \frac{f(\{(\mathbf{y}_1, \mathbf{u}_1), \dots, (\mathbf{y}_k, \mathbf{u}_k), (\mathbf{y}, \mathbf{u})\} | \{\mathbf{x}_1, \dots, \mathbf{x}_n\}, \alpha, \sigma^2, \rho_L, \boldsymbol{\mu}, \kappa)}{f(\{(\mathbf{y}_1, \mathbf{u}_1), \dots, (\mathbf{y}_k, \mathbf{u}_k)\} | \{\mathbf{x}_1, \dots, \mathbf{x}_n\}, \alpha, \sigma^2, \rho_L, \boldsymbol{\mu}, \kappa)} \times \frac{1/(k+1)}{f(\mathbf{y}, \mathbf{u} | \boldsymbol{\mu}, \kappa)} \\ &= \frac{2\pi^{d/2}}{\Gamma(d/2)} \rho_L f(\mathbf{u} | \boldsymbol{\mu}, \kappa) \mathbf{1}[\mathbf{y} \in J_{\mathbf{u}}] \frac{1}{(k+1) f(\mathbf{y}, \mathbf{u} | \boldsymbol{\mu}, \kappa)} \\ &\quad \times \exp\left(-\alpha \int_W f(p_{\mathbf{u}^\perp}(\mathbf{x} - \mathbf{y}) | \sigma^2) d\mathbf{x}\right) \prod_{i=1}^n \left(1 + \frac{f(p_{\mathbf{u}^\perp}(\mathbf{x}_i - \mathbf{y}) | \sigma^2)}{\sum_{j=1}^k f(p_{\mathbf{u}_j^\perp}(\mathbf{x}_i - \mathbf{y}_j) | \sigma^2)}\right) \end{aligned}$$

which is equal to (28). Thereby, referring again to Geyer and Møller (1994), we obtain (29).

References

- Baddeley, A. & Turner, R. (2005). Spatstat: an R package for analyzing spatial point patterns. *Journal of Statistical Software* **12**, 1–42.
- Baddeley, A., Møller, J. & Waagepetersen, R. (2000). Non- and semi-parametric estimation of interaction in inhomogeneous point patterns. *Statistica Neerlandica* **54**, 329–350.
- Chiu, S. N., Stoyan, D., Kendall, W. S. & Mecke, J. (2013). *Stochastic Geometry and Its Applications*. John Wiley and Sons, Chichester.
- Diggle, P., Chetwynd, A., Häggkvist, R. & Morris, S. (1995). Second order analysis of space-time clustering. *Statistical Methods in Medical Research* **4**, 124–136.
- Diggle, P. J. & Gratton, R. (1984). Monte Carlo methods of inference for implicit statistical models. *Journal of the Royal Statistical Society: Series B (Statistical Methodology)* **46**, 193–212.
- Gabriel, E. & Diggle, P. (2009). Second-order analysis of inhomogeneous spatio-temporal point process data. *Statistica Neerlandica* **63**, 43–51.
- Geyer, C. & Møller, J. (1994). Simulation procedures and likelihood inference for spatial point processes. *Scandinavian Journal of Statistics* **21**, 359–373.

- Gilks, W. R., Richardson, S. & Spiegelhalter, D. (1996). *Markov Chain Monte Carlo in Practice*. Chapman and Hall, London.
- Guan, Y. (2006). A composite likelihood approach in fitting spatial point process models. *Journal of the American Statistical Association* **101**, 1502–1512.
- Illian, J., Penttinen, A., Stoyan, H. & Stoyan, D. (2008). *Statistical Analysis and Modelling of Spatial Point Patterns*. John Wiley and Sons, New York.
- Møller, J. & Toftaker, H. (2014). Geometric anisotropic spatial point pattern analysis and Cox processes. *Scandinavian Journal of Statistics* **41**, 414–435.
- Møller, J. & Waagepetersen, R. (2004). *Statistical Inference and Simulation for Spatial Point Processes*.
- Møller, J. & Waagepetersen, R. (2007). Modern statistics for spatial point processes (with discussion). *Scandinavian journal of Statistics* **34**, 643–711.
- Mountcastle, V. B. (1957). Modality and topographic properties of single neurons of cat's somatic sensory cortex. *Journal of Neurophysiology* **20**, 408–434.
- Muggleston, M. & Renshaw, E. (1996). A practical guide to the spectral analysis of spatial point processes. *Computational Statistics & Data Analysis* **21**, 43–65.
- Myllymäki, M., Mrkvička, T., Seijo, H. & Grabarnik, P. (2013). Global envelope tests for spatial processes. Available at arXiv:1307.0239.
- Neyman, J. & Scott, E. L. (1958). Statistical approach to problems of cosmology. *Journal of the Royal Statistical Society: Series B (Statistical Methodology)* **20**, 1–29.
- Nicolis, O., Mateu, J. & Dercole, R. (2010). Testing for anisotropy in spatial point processes. In: *Proceedings of the Fifth International Workshop on Spatio-Temporal Modelling (METMA5)* (ed. G.-M. et al.), Unidixital.
- Ohser, J. & Stoyan, D. (1981). On the second-order and orientation analysis of planar stationary point processes. *Biometrical Journal* **23**, 523–533.
- Rafati, A., Safavimanesh, F., Dorph-Petersen, K., Rasmussen, J. G., Møller, J. & Nyengaard, J. R. (2015). Detection and spatial characterization of minicolumnarity in the human cerebral cortex. Submitted for publication.
- Redenbach, C., Särkkä, A., Freitag, J. & Schladitz, K. (2009). Anisotropy analysis of pressed point processes. *ASTA Advances in Statistical Analysis* **93**, 237–261.
- Ripley, B. D. (1976). The second-order analysis of stationary point processes. *Journal of Applied Probability* **13**, 255–266.
- Ripley, B. D. (1977). Modelling spatial patterns (with discussion). *Journal of the Royal Statistical Society: Series B (Statistical Methodology)* **39**, 172–212.
- Roberts, G. O., Gelman, A. & Gilks, W. R. (1997). Weak convergence and optimal scaling of random walk Metropolis algorithms. *Annual of Applied Probability* **7**, 110–120.
- Rosenberg, M. S. (2004). Wavelet analysis for detecting anisotropy in point patterns. *Journal of Vegetation Science* **15**, 277–284.
- Safavimanesh, F. & Redenbach, C. (2015). On the functional summary statistics for detecting anisotropy of three-dimensional spatial point patterns. Manuscript in preparation.
- Stoyan, D. (1991). Describing the anisotropy of marked planar point process. *Statistics: A Journal of Theoretical and Applied Statistics* **22**, 449–462.
- Stoyan, D. & Beneš, V. (1991). Anisotropy analysis for particle systems. *Journal of Microscopy* **164**, 159–168.

Stoyan, D. & Stoyan, H. (1995). *Fractals, Random Shapes and Point Fields*. John Wiley and Sons, Chichester.